Nickel ferrite nanoparticles catalyzed dark fermentation of dairy wastewater for biohydrogen production

Fahoul, Nazanin; Sayadi, Mohammad Hossein; Reza Rezaei, Mohammad; Homaeigohar, Shahin

DOI:
10.1016/j.biteb.2022.101153

Publication date:
2022

Journal Pre-proof

Nickel ferrite nanoparticles catalyzed dark fermentation of dairy wastewater for biohydrogen production

Nazanin Fahoul, Mohammad Hossein Sayadi, Mohammad Reza Rezaei, Shahin Homaeigohar

PII: S2589-014X(22)00210-9

DOI: https://doi.org/10.1016/j.biteb.2022.101153

Reference: BITEB 101153

To appear in: *Bioresource Technology Reports*

Received date: 20 May 2022

Revised date: 5 July 2022

Accepted date: 6 July 2022

Please cite this article as: N. Fahoul, M.H. Sayadi, M.R. Rezaei, et al., Nickel ferrite nanoparticles catalyzed dark fermentation of dairy wastewater for biohydrogen production, *Bioresource Technology Reports* (2022), https://doi.org/10.1016/j.biteb.2022.101153

Nickel ferrite nanoparticles catalyzed dark fermentation of dairy wastewater for biohydrogen production

Nazanin Fahoul [1], Mohammad Hossein sayadi *[1], Mohammad Reza Rezaei [1], Shahin Homaeigohar [2]

[1]Department of Environmental Engineering, Faculty of Natural Resources and Environment, University of Birjand, Birjand, Iran

[2] School of Science and Engineering, University of Dundee, DD1 4HN, UK

Corresponding author: * Mh_sayadi@birjand.ac.ir

Abstract:

Biohydrogen production from wastewater is a new, low cost, sustainable energy development. In this study, dark fermentation, as a type of biological production of biohydrogen, was carried out using $NiFe_2O_4$ nanoparticle catalysts. Implementing the Central Composite Design model, the operational parameters including temperature, pH, and nanoparticle dosage were optimized. According to the spectroscopic and microscopic analyses, $NiFe_2O_4$ nanoparticles were successfully synthesized. The highest biohydrogen amount, i.e., ~241.5 mL, was obtained at 36 °C, 300 mg/L catalyst dosage, pH6.5, and within the time range of 12 to 24 hours. The biochemical oxygen demand and chemical oxygen demand were measured to be 153 and 87 mg/L, respectively, which were 97.5 and 83.6% lower than their initial values. The $NiFe_2O_4$ nanoparticles could properly act as a catalyst for the dark fermentation process and promote the expression of the hydrogenase enzyme in bacterial cells, thereby producing a higher amount of biohydrogen.

Keywords: Hydrogenase, Nanomaterials, H_2 generation, Nanocatalysts.

1. Introduction

In recent decades, increasing population and industrialization have led to a higher demand for fossil fuels, thus unbalancing the energy resources in the world (Xia, A., et al.,2016). This situation has also engendered larger emission of greenhouse gases such as CH_4, NO_x, CO_2, SO_2 and other environmental problems such as global warming (Tasleem et al., 2021). Therefore, development of clean and renewable energy resources is essential to reduce such environmental concerns (Chen et al., 2019). Hydrogen is a promising alternative for fossil fuels and considered as a renewable, clean, and high-energy (equivalent to 142 MJ per kilogram, which is 2.75 times higher than that of hydrocarbon fuels) source (Mallikarjuna et al., 2021). Currently, 96% of hydrogen worldwide is produced mainly through fossil fuels and only 4% through the electrolysis of water (Capurso et al., 2022). The main hydrogen production methods based on renewable sources include: water fission (electrolysis, thermolysis, radiolysis, and photolysis of water), and biological (Mallikarjuna et al., 2021), thermochemical (pyrolysis and gasification), photoelectrochemical, photochemical, and photocatalytic processes (Nanda et al., 2017, Agyekum et al., 2022). Among them, biological methods (dark fermentation and light fermentation) are the most favorable due to their environmentally friendliness and low energy consumption. These techniques produce hydrogen from waste materials at ambient temperature and pressure (Sigal et al., 2014). Regarding dark fermentation, pure and stable hydrogen is easily derived from waste precursors (Rittmann and Herwig, 2012). This method is in fact a low cost technology with no need to light and oxygen, operating based on a high microbial growth

rate (Ziara et al., 2019, Rittmann and Herwig, 2012). However, there are also several limitations such as the need to costly bioreactors, low hydrogen production rate, stunted growth, and reactor instability in continuous hydrogen production (Das et al., 2014).

As a solution for the aforementioned bottlenecks in biohydrogen production by dark fermentation, nanotechnology, and particularly the use of nanoparticle catalysts, have been shown to be promising. Thanks to their small size and large surface to volume ratio, nanoparticles stimulate the biological activity of microbes (Ramprakash and Incharoensakdi, 2020), thereby enhancing the biogas production efficiency in dark fermentation systems (Zhang and Shen, 2007), The biological activity of microbes is mainly stimulated by electron transfer (Lin et al., 2016) and upregulation of the hydrogenase gene in the presence of nanoparticles (Hsieh et al., 2016). Hydrogenase is a key cellular enzyme in hydrogen production pathways and during the transmission process. It properly converts electrons to hydrogen ions, thereby acting as a catalyst in the dark fermentation process, enabling a higher hydrogen production rate (Patel et al., 2018). In this regard, recently, Fe_2O_3 (Lin et al., 2016), ZnO (Liu et al., 2017), TiO_2 (Abdul et al., 2020), and $CoFe_2O_4$ (Zhang et al., 2021) nanoparticles have been employed as a catalyst.

Metal nanoparticles, such as those made of iron (Fe) and nickel (Ni), play an important role as macro- and micronutrients in microbial growth and metabolic activities of microbes, thereby improving hydrogen production efficiency (Budiman and Wu, 2018). Fe and Ni serve as a metal cofactor and increase the catalytic activity of hydrogenase (Srivastava et al., 2019). Ni supports the activity of ferredoxin oxidoreductase by promoting the electron transfer rate, thus the hydrogenase activity (Gadhe et al., 2015). Because of its high excitability, Fe also binds to ferredoxin in the enzyme as an electron carrier (Budiman and Wu 2018) and speeds up the electron transfer rate during the hydrogen production cycle (Tiang et al., 2020). Benefiting from the synergistic catalytic activity of Fe and Ni, in the present study, for the first time, contribution of $NiFe_2O_4$ nanoparticles to production of biohydrogen from a real dairy wastewater and active sludge was investigated. In this regard, the Central Composite Design model from the response surface models was applied to optimize the operational parameters of the dark fermentation process including temperature, pH, and nanoparticle dosage.

2. Materials and Methods

2.1. Materials

Fe_3O_4 nanoparticle (98%), $NiCl_2.6H_2O$ (99.99%), polyethylene glycol (PEG 6000), and NaOH (98%) were purchased from Merck, Germany. HCl , deionized water, and ethanol for washing nanoparticles.

2.2. Synthesis of $NiFe_2O_4$ nanoparticles

To synthesize $NiFe_2O_4$ nanoparticles, Fe_3O_4 nanoparticles (2.3 g) and $NiCl_2.6H_2O$ (2.9 g) were dispersed in deionized water (100 mL). In the next step, PEG (0.5 g) and NaOH (1 M) were gradually added to the suspension, while being heated (50 °C) on a heater (Mtops Ms300hs Magnetic Stirrer, Korea) and stirred with a magnetic stirrer at 140 rpm. Throughout the preparation process, pH was precisely controlled to be $12 \leq pH \leq 13$. Finally, the synthesized nanoparticles were washed with water and ethanol and dried in an oven (RTC, nv_SD9002) at 80 °C for 24 hours (Farooghi et al.,2018).

2.3. Characterization

To identify the crystalline structure of the synthesized nanoparticles, X-ray diffraction analysis (XRD, Rigaku Ultima IV) was carried out. The optical property of the nanoparticles was determined using a UV-vis Spectrophotometer (Shimadzu, UV-160 A). Surface chemical analysis was performed using X-ray photoelectric spectroscopy (XPS, VG ESCALAB 210 electron spectrometer). Field emission scanning electron microscopy (FESEM, ZEISS Sigma 300) was also used to identify the shape and size of the nanoparticles. Element composition of the samples was analyzed by Energy Dispersive X-ray spectroscopy.

2.4. Preparation of microbial strains

The Escherichia coli bacteria strain (ATCC: 25922; Pasteur Institute of Tehran) was cultured in 10 plates containing eosin methylene blue (EMB) via the linear culture method. The bacteria grown in the incubator (INFORS AG CH-4103 Botteringan) were then incubated for 24 hours at 38 °C and used for further experiments.

2.5. Characterization of dairy wastewater and activated sludge

Dairy wastewater and activated sludge were collected from the Nimblok dairy factory (Birjand, Iran) and used as a substrate. Table 1 shows the physicochemical characteristics of the dairy wastewater including COD (measured via the standard open reflux method), TSS (measured by a TSS meter (LAV, 3229900002)), BOD (measured by a BOD meter (OxiTop IS6)), and pH (measured by a pH meter (Istek 915P DC)).

Table 1. physicochemical characteristics of the Nimblok dairy wastewater

Parameters	**dairy wastewater**	**activated sludge**
pH	7	7.8
Color	brown	gray
COD (mg/L)	45	705
BOD (mg/L)	5056	331
TDS (mg/L)	2400	1195
TSS (mg/L)	1100	367.6

2.6. Optimization of operational parameters

All initial optimization studies were carried out using Response Surface Methodology (RSM) in the Design–Expert 7.0.0 software environment. RSM is a statistical empirical technique that determines the significance of parameters by a factorial method (Rafiee and Bashiri, 2020). Three parameters of temperature, pH, and concentration of $NiFe_2O_4$ nanoparticles were selected as the optimization parameters, and 20 runs was chosen as the number of experiment repetitions to examine the parameters' effects. Later, 20 vials (50 mL) containing one colony of E. coli, 25 mL of the dairy wastewater, and different concentrations of nanoparticles (100, 200, 300, 400, and 500 mg/L) were prepared. The pH of the media was adjusted to be 4, 5, 6.5, 8, and 9, using HCl (1M) and NaOH (1M). The temperature of the media adjusted to be 27, 30, 36, 42, and 45 °C. Finally, all 20 vials were incubated for 24 hours in the dark. Thereafter, the amount of the released hydrogen was measured. Eventually, based on the optimized parameters and by using 25 mL of industrial dairy (as the carbon source) and 25 mL of active sludge (as the microbial community), the amount of the produced hydrogen

was quantified. It is worthy to note that bottles with rubber septum and sealed screw caps were used for testing. The bottles were placed in the incubator in the dark. The H2 production in the bottle cap spade was measured after 48 hours by gas chromatography.

3. Results and discussion

3.1. Characterization of $NiFe_2O_4$ nanoparticles

3.1.1. XRD

The XRD spectrum of the $NiFe_2O_4$ nanoparticles compared to the standard spectrum (JCPDS Card No. 37-0474) is shown in Supporting Material (SM1a). The characteristic diffraction peaks appearing at $2\theta = 44^\circ$, 51°, and 76°, represent the (111), (200), and (222) crystalline planes of $NiFe_2O_4$ nanoparticles, respectively. Compliance of the two spectra ($NiFe_2O_4$ nanoparticles and the standard) implies the presence of Fe and Ni in the synthesized nanoparticles (Kumari et el., 2021, Shekari et al., 2017).

3.1.2. Optical properties

The optical properties of the $NiFe_2O_4$ nanoparticles were determined through UV–Vis spectroscopy. SM1b shows that the absorption peak of the nanoparticles is located at $\lambda = 270$ nm and 291 nm. This absorption spectrum indicates the d-d transfer that corresponds to the octahedral Ni^{2+}. This electronic transition in the complex of nickel and iron is associated with $^3A_{2g} \rightarrow {}^3T_{1g}$ (P) and results in an increase in the catalytic activity of the nanoparticle (Jaśkaniec et al., 2018). Additionally, the absorption peak is located within the visible light region, implying the possibility of solar light absorption of the nanoparticles (Chamanehpour et al.,2022).

3.1.3. XPS

SM1c illustrates the general XPS spectrum of the nanoparticles including O1s, C1s, Fe 2p, and Ni 2p peaks. SM1d also shows Fe 2p XPS pattern that clearly indicates the presence of Fe in the synthesized nanoparticles. The spectrum contains two bands attributed to Fe 2p1/2 (725 eV) and Fe 2p3/2 (710.6 eV) photoelectrons. The peak emerging at 710.6 eV represents the presence of Fe^{3+} cations (Fan et al., 2020). The peaks appearing at 706.9 and 719.5 eV can be assigned to Fe0 2p3/2 (Tiang et al., 2020, Rafiee and Bashiri, 2020). Ni 2p XPS pattern (SM1e) includes the Ni characteristic peaks at 856.1 eV and 874.9 eV representing NiO, and the peaks at 881.2 eV and 861.9 eV representing Ni^{2+} (Nguyen et al., 2018).

3.1.4. Morphology and elemental composition

According to the FESEM micrographs (SM2a), the nanoparticles are as small as 67±19 nm in diameter and almost spherical. The nanoparticles are highly aggregated mainly due to strong magnetic interaction between the two metals (Ezzatahmadi et al., 2019). EDS analysis (SM2b), verifies the co-existence of Fe, Ni, C, and O in $NiFe_2O_4$ nanoparticles, as similarly shown by XPS.

3.2. Design and optimization of experimental parameters using RSM

The optimization of the experimental parameters was carried out using the central composite design (CCD) model from a series of response surface method (RSM) models (Rhazi et al., 2019). Table 2 tabulates the experimental results of CCD, which match well with those anticipated by the model.

Table 2. CCD optimized parameters.

Run	Catalyst dosage (mg/L)	Temperature (ºC)	pH	Actual amount of produced H_2 (mL)	Predicted amount of produced H_2 (mL)
control	0	36	6.5	11.03	10.09
1	400	30	8	205	206.2
2	100	30	5	194.4	193.1
3	300	36	6.5	253.1	246.9
4	400	36	6.5	231	239.0
5	400	42	5	222.7	220.5
6	300	36	6.5	249.8	246.9
7	100	42	8	191.5	188.5
8	300	36	5	225.9	236.5
9	400	30	5	208	209.5
10	100	42	5	193.7	190.9
11	100	30	8	192.3	191.1
12	400	42	8	219.1	217.2
13	300	36	6.5	251.5	235.1
14	300	36	9	201.9	200.5
15	300	36	4	207.5	205.2
16	300	36	8	212.8	222.1
17	500	36	6.5	206.6	204.1
18	300	45	6.5	203.4	208.8
19	300	27	6.5	199.8	198.8
20	200	36	6.5	195.9	204.9

The most optimum model for data fitting is quadratic. To investigate the adequacy of the model, ANOVA analysis and residuals normal plot and versus plot were used sequentially. When p-value of the model is less than 0.05 and lack of fit is over 0.05, the model is significantly reliable at the 95% level. As seen in Table 3, R2 and adjusted R2 values obtained by this model are equal to 0.9 and 0.8, respectively. Thus, the experimental data fit well with the quadratic model. Table 4, tabulating the results of ANOVA, also indicates that there is a good match between the actual and predicted amount of the produced H_2 via the quadratic model.

Table 3. evaluation of the reliability of the quadratic model in prediction of optimal H_2 production parameters.

Response	Analysis	Min	Max	Mean	Model	p-value	R^2	Adjusted R^2
H_2 production (R1)	Polynomial	191.5	253.1	213.3	Quadratic	0.0003	0.90	8

Table 4. The results of analysis of variance (ANOVA)

Source	Sum of Squares	Mean Square	F-value	p-value
Model	6630.8	736.8	9.04	0.001
A-catalyst dose	0.73	0.73	0.009	0.920
B-Tem.	130.4	130.4	1.6	0.230
C-pH	30.19	30.19	0.37	0.500
AB	95.42	95.42	1.17	0.300
AC	0.67	0.67	0.008	0.100
BC	0.06	0.06	0.0008	0.100
A^2	2261.8	2261.8	27.75	0.001
B^2	1929.2	1929.2	23.67	0.001
C^2	1703.8	1703.8	20.9	0.001

Fig. 1a implies the normality of the data, given all data points are almost on a straight line. Other than a few data points, majority do not exceed the residual variance, thus indicating the adequacy of the regression model. Fig. 1b shows that the predicted responses follow a random distribution mode and the variance is constant as the values lie between the two red lines. The residual versus predicted diagram shows that the difference between the predicted and actual values is negligible and the model provides a good fit. This reality is also confirmed by the predicted versus actual chart (Fig. 1c). Fig. 1d represents the autonomy of the data over time because no particular trend is observed in the graph.

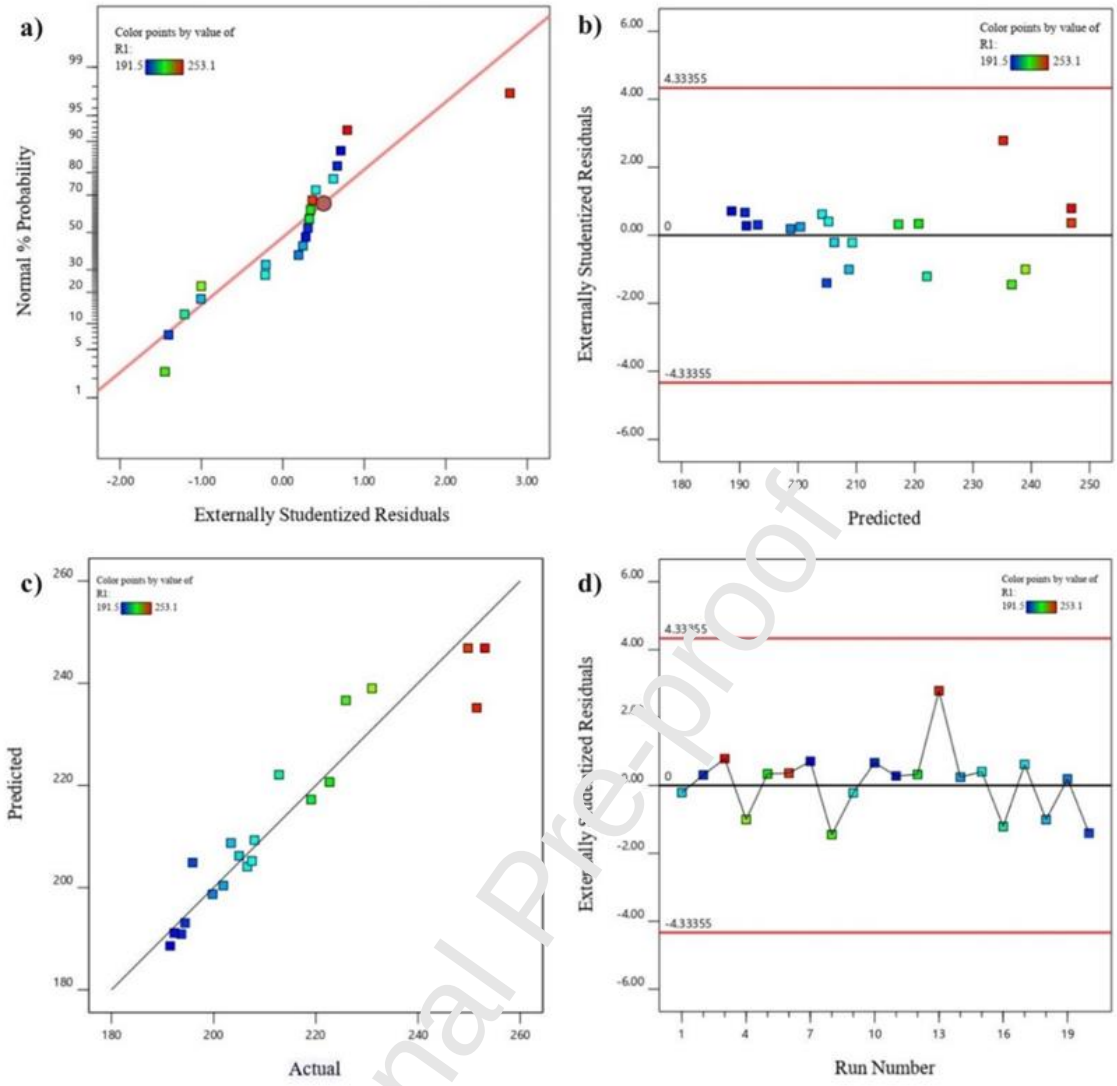

Figure 1. a) normal plot of residuals, b) residual versus predicted plot, c) predicted versus actual plot, and d) residual versus run plot.

Considering the outputs of the CCD model, the most optimum experimental conditions for H_2 production (241.273 mL) included: a colony of E. Coli, 25 mL of dairy wastewater, a nanoparticle dosage of 300 mg/L, pH 6.5, temperature of 36 °C, and a Media volume of 50mL.

In the next step, to investigate the correlation between the experimental parameters and the amount of produced H_2, three-dimensional (3D) plots were constructed. In these graphs, two factors vary and one factor is kept at the center point to show the reciprocal effect of two other factors on the amount of produced H_2 (Salarian et al., 2016). The curve in the diagram shows the best mode. The interaction between temperature and nanoparticle dosage, pH and nanoparticle dosage, and temperature and pH is shown in Fig2a-c, respectively. With increasing the nanoparticle dosage up to 300 mg, hydrogen production also increases. The reason for this behaviour can be entrapment of oxygen electrons by the nanoparticles, resulting in generation of a larger number of free radicals and thus increased hydrogen production (Yi et al., 2021). Over this critical nanoparticle dosage, hydrogen production declines. This reduction can be attributed to the imbalance between the amount of free radicals and present antioxidants in the cell, which can lead to inflammatory

reactions and death of microorganisms. This oxidative stress leads to the impaired physiological function of microorganisms (Yin and Wang,2019).

This performance and trend in production of hydrogen is similarly seen when temperature changes. The highest hydrogen yield is observed at 36 °C, in which the highest growth rate and microbial activity are available. Other studies have also reported an optimum temperature range of 25 to 37°C for Escherichia coli. At temperatures more or less than the optimum temperature range, the microorganism loses its control mechanism (Adler and Templeton,1967). The pH variation affects in analogue to temperature and nanoparticle dosage. The optimum pH is 6.5, where bacteria have the highest enzyme activity. The pH change impacts the ligand bonds of the enzyme. As validated earlier, the most optimum pH for enzymatic activity is between 6 and 8 (Trchounian et al., 2013).

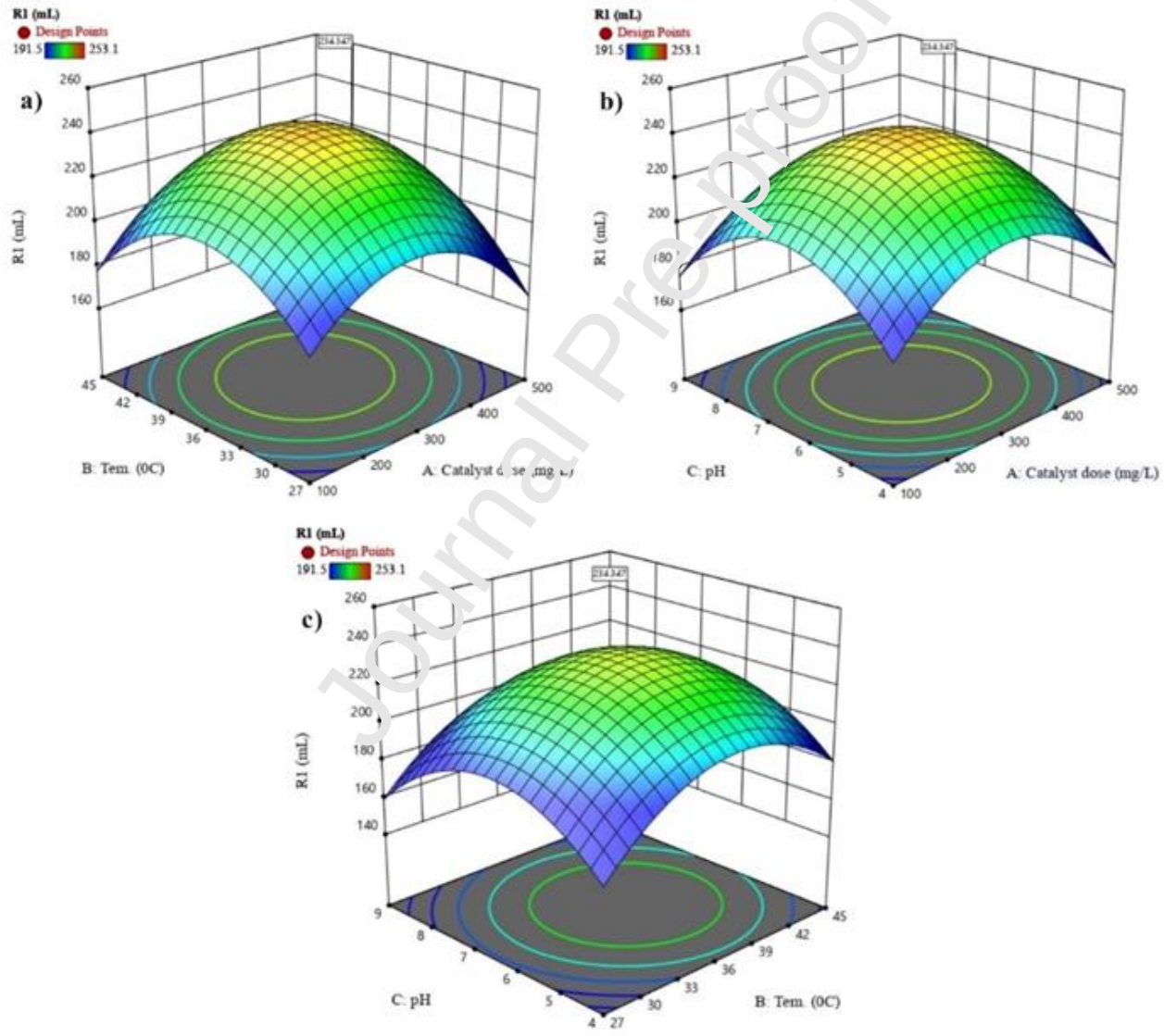

Figure 2. Response surface result of quadratic model for $NiFe_2O_4$ nanoparticle catalyzed biohydrogen production considering the mutual effect of a) temperature and catalyst dosage, b) pH and catalyst dosage, and c) pH and temperature.

3.3. Hydrogen production

Having determined the most optimum experimental parameters, hydrogen production experiment was carried out via dark fermentation, involving activated sludge (microbial community) and dairy wastewater (carbon source). Fig. 3 shows that the quantity of the produced hydrogen in the first 12h is not so high as bacteria are still in the delayed phase (lag). Thereafter, the quantity rises significantly with exponential growth of bacteria (phase log). The highest amount of hydrogen is produced between 12 and 24 hours. Afterwards, bacteria enter a static stage in which the amount of substrate nutrients is limited and organic acids are produced (Łukajtis et al., 2018).

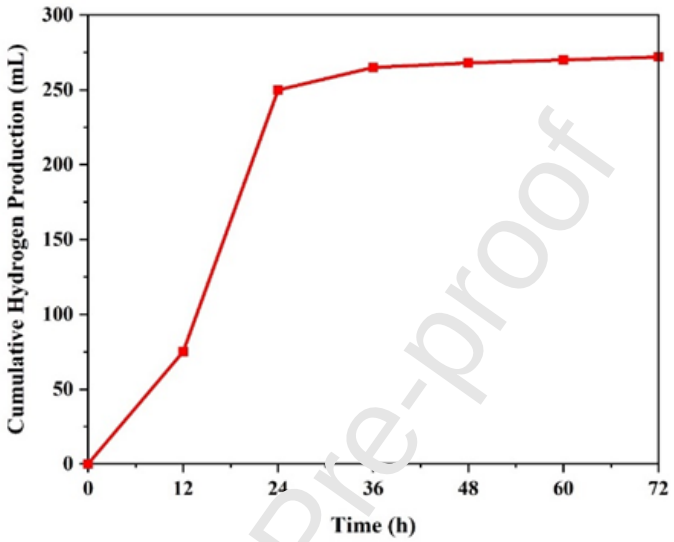

Figure 3. Cumulative hydrogen production under optimum conditions determined through the CCD model.

It should be noted that $NiFe_2O_4$ nanoparticles act as a supplement and encourage the expression of the hydrogenase enzyme in bacteria. As a result, electron transfer rate in the redox reaction is enhanced and oxygen in the fermentation medium is consumed to generate free radicals (reaction 1), thereby increasing the amount of the produced hydrogen (Rambabu et al., 2021).

Reaction 1: $NPs + O_2 \rightarrow ROS(O_2^- + H_2O_2)$

The available glucose in the substrate can be fermented in different ways and converted to hydrogen. The most important byproducts include acetic acid (CH_3COOH), butyric acid ($CH_3CH_2CH_2COOH$), and ethanol (CH_3CH_2OH) (reaction 2-4) (Song et al., 2020):

Reaction 2: $C_6H_{12}O_6 + 4H_2O \rightarrow 4H_2 + 2CH_3COOH + 2CO_2$ ($\Delta G_0 = -206$ kJ)

Reaction 3: $C_6H_{12}O_6 + 2H_2O \rightarrow 2H_2 + CH_3CH_2CH_2COOH + 2CO_2$ ($\Delta G_0 = -254$ kJ)

Reaction 4: $C_6H_{12}O_6 + 3H_2O \rightarrow CH_3OO^- + 2HCO_3^- + 3H^+ + CH_3CH_2OH$ ($\Delta G_0 = -97$ kJ/mol)

3.4. Wastewater treatment under optimum conditions

As shown in table 5, $NiFe_2O_4$ nanoparticles can decompose organic pollutants of wastewater streams (here a combination of diary wastewater and activated sludge), represented by variation of COD and BOD (Xu et al., 2019). As recorded in our experiment, BOD declined to 153 mg/L from 5956 mg/L, which is 97.5% lower than the primary level. Also, COD decreased by 83.6 % to 87 mg/L. Thus, the synthesized nanoparticles are bifunctional and not only help produce

biohydrogen, but also decontaminate wastewater streams. This behaviour has been similarly reported by other researchers. For instance, (Dlamini et al., 2020) used iron chloride nanoparticles in treatment of domestic wastewater, thereby reducing COD and BOD by 81% and 72%, respectively. Chaurasia and Mondal also validated high pollutant removal efficiency of Ni and Ni-Co nanoparticles for wastewaters of sugar industries with high COD and BOD (Chaurasia and Mondal, 2022).

Table 5. The COD and BOD characteristic of wastewater before and after $NiFe_2O_4$ nanoparticle catalyzed dark fermentation

Parameters	Before dark fermentation	After dark fermentation	Removal percentage
COD	530mg/L	87.5mg/L	83.6%
BOD	5956mg/L	148.9mg/L	97.5%

4. Conclusions

In the present study, an industrial dairy wastewater was employed for production of biohydrogen via dark fermentation catalyzed by $NiFe_2O_4$ nanoparticles. The operational parameters were optimized using the CCD model. The optimized process was driven by further expression of hydrogenase in the bacteria within the activated sludge in the presence of the nanoparticles. The nanoparticle catalyst dosage affects the generation of oxidative stress, while temperature and pH modulate bacterial growth and activity, and expression of cellular enzymes, respectively. On the whole, the nanoparticle catalyzed dark fermentation was shown to be effective in sustainable production of biohydrogen.

CRediT authorship contribution statement

N. Fahul: Investigation, Visualization, Writing – original draft. **M.H. Sayadi:** Investigation, Conceptualization, Funding acquisition, Supervision, Writing - review & editing. **M.R. Rezaei:** Method development, Writing – review & editing. **S. Homaeigohar:** Investigation, Conceptualization, Supervision, Writing – review & editing.

Declaration of competing interest

The authors declare that they have no known competing financial interests or personal relationships that could have appeared to influence the work reported in this paper

Acknowledgments: This paper is based on the results of a postgraduate student thesis (ID Number: 8542/1400) undertaken at the department of environmental engineering, Faculty of Natural Resources and Environment, University of Birjand. N.F., M.H.S., and M.R.R. gratefully acknowledge the kind cooperation of the personnel of the laboratories, Faculty of Natural Resources and Environment, University of Birjand, over the course of the research.

References

Abdul, S., Mahadi, A. H., Abdullah, R., Yasin, H. M., Ja'afar, F., Abdul Rahman, N., Bahruji, H., 2020. Biohydrogen production from photodecomposition of various cellulosic biomass wastes using metal-TiO_2 catalysts. Biomass Convers. Biorefin. 1–12. https://doi.org/10.1007/s13399-020-01164-4

Adler, J., Templeton, B., 1967. The effect of environmental conditions on the motility of Escherichia coli. Microbiology, 46, 175–184. https://doi.org/10.1099/00221287-46-2-175

Agyekum, E. B., Nutakor, C., Agwa, A. M., Kamel, S., 2022. A Critical Review of Renewable Hydrogen Production Methods: Factors Affecting Their Scale-Up and Its Role in Future Energy Generation. Membranes, 12(2), 173. https://doi.org/10.3390/membranes12020173

Budiman, P. M., Wu, T. Y., 2018. Role of chemicals addition in affecting biohydrogen production through photofermentation. Energy Convers. Manag.165, 509–527. https://doi.org/10.1016/j.enconman.2018.01.058

Capurso, T., Stefanizzi, M., Torresi, M., Camporeale, S. M., 2022. Perspective of the role of hydrogen in the 21st century energy transition. Energy Convers. Manag. 251, 114898. https://doi.org/10.1016/j.enconman.2021.114898

Chamanehpour, E., Sayadi, M. H., Hajiani, M., 2022. A hierarchical graphitic carbon nitride supported by metal–organic framework and copper nanocomposite as a novel bifunctional catalyst with long-term stability for enhanced carbon dioxide photoreduction under solar light irradiation. Adv. Compos. Mater. 1–17. https://doi.org/10.1007/s42114-022-00459-6

Chaurasia, A. K., Mondal, P., 2022. Enhancing biohydrogen production from sugar industry wastewater using Ni, Ni–Co and Ni–Co–P electrodeposits as cathodes in microbial electrolysis cells. Chemosphere, 286, 131728. https://doi.org/10.1016/j.chemosphere.2021.131728

Chen, H., Wu, J., Liu, B., Li, Y., Yasui, H., 2019. Competitive dynamics of anaerobes during long-term biological sulfate reduction process in a UASB reactor. Biores.Technol. 280, 173–182. https://doi.org/10.1016/j.biortech.2019.02.023

Das, D., Khanna, N., Dasgupta, C., 2014. Biohydrogen Production. CRC Press.

Dlamini, N. G., Basson, A. K., Pullabhotla, V. S. R., 2020. Biosynthesis of bioflocculant passivated copper nanoparticles, characterization and application. Phys. Chem. Earth, 118, 102898. https://doi.org/10.1016/j.pce.2020.102898

Ezzatahmadi, N., Millar, G. J., Ayoko, G. A., Znu, J., Zhu, R., Liang, X., He, H., Xi, Y., 2019. Degradation of 2, 4-dichlorophenol using palygorskite-supported bimetallic Fe/Ni nanocomposite as a heterogeneous catalyst. Appl. Clay Sci. 168, 276–286. https://doi.org/10.1016/j.clay.2018.11.030

Fan, L., Xie, J., Zhang, Z., Zheng, Y., Yao, D., Li, T., 2020. Magnetically recoverable Fe3O4@ polydopamine nanocomposite as an excellent co-catalyst for Fe^{3+} reduction in advanced oxidation processes. J. Environ. Sci. 92, 69-78. https://doi.org/10.1016/j.jes.2020.02.006

Farooghi, A., Sayadi, M. H., Rezaei, M. R., Allahresani, A., 2018. An efficient removal of lead from aqueous solutions using $FeNi_3$@ SiO_2 magnetic nanocomposite. Surf. Interfaces, 10, 58–64. https://doi.org/10.1016/j.surfin.2017.11.005

Gadhe, A., Sonawane, S. S., Varma, M. N., 2015. Enhancement effect of hematite and nickel nanoparticles on biohydrogen production from dairy wastewater. Int. J. Hydrog. Energy, 40(13), 4502–4511. https://doi.org/10.1016/j.ijhydene.2015.02.046

Hsieh, P.-H., Lai, Y.-C., Chen, K.-Y., Hung, C.-H., 2016. Explore the possible effect of TiO2 and magnetic hematite nanoparticle addition on biohydrogen production by Clostridium pasteurianum based on gene expression measurements. Int. J. Hydrog. Energy, 41(46), 21685–21691. https://doi.org/10.1016/j.ijhydene.2016.06.197

Jaśkaniec, S., Hobbs, C., Seral-Ascaso, A., Coelho, J., Browne, M. P., Tyndall, D., Sasaki, T., Nicolosi, V., 2018. Low-temperature synthesis and investigation into the formation mechanism of high quality Ni-Fe layered double hydroxides hexagonal platelets. Sci. Rep. 8(1), 1–8. https://doi.org/10.1038/s41598-018-22630-0

Kumari, K., Kumar, A., Lee, J. E., Koo, B. H., 2021. Investigating the origin of exchange bias effect in ferromagnetic FeNi nanoparticles prepared via controlled synthesis. Appl. Nanosci. 1–9. https://doi.org/10.1007/s13204-021-01870-z

Lin, R., Cheng, J., Ding, L., Song, W., Liu, M., Zhou, J., Cen, K., 2016. Enhanced dark hydrogen fermentation by addition of ferric oxide nanoparticles using Enterobacter aerogenes. Bioresour. Technol. 207, 213–219. https://doi.org/10.1016/j.biortech.2016.02.009

Liu, B., Jin, Y., Wang, Z., Xing, D., Ma, C., Ding, J., Ren, N., 2017. Enhanced photo-fermentative hydrogen production of Rhodopseudomonas sp. nov. strain A7 by the addition of TiO_2, ZnO and SiC nanoparticles. Int. J. Hydrog. Energy, 42(29), 18279–18287. https://doi.org/10.1016/j.ijhydene.2017.04.147

Łukajtis, R., Hołowacz, I., Kucharska, K., Glinka, M., Rybarczyk, P., Przyjazny, A., Kamiński, M., 2018. Hydrogen production from biomass using dark fermentation. Renew. Sust. Energ. Rev. 91, 665–694. https://doi.org/10.1016/j.rser.2018.04.043

Mallikarjuna, K., Nasif, O., Ali Alharbi, S., Chinni, S. V, Reddy, [illegible] V. Reddy, M. R. V., Sreeramanan, S., 2021. Phytogenic synthesis of Pd-Ag/rGO nanostructures using stevia leaf extract for photocatalytic H_2 production and antibacterial studies. Biomolecules, 11(2), 190. https://doi.org/10.3390/biom11020190

Nanda, S., Rana, R., Zheng, Y., Kozinski, J. A., Dalai, A. K., 2017. Insights on pathways for hydrogen generation from ethanol. Sustain. Energy Fuels, 1(6), 1232–1245. https://doi.org/10.1039/C7SE00212B

Nguyen, V. H., Nguyen, T. D., Bach, L. G., Hoang, T., Bui, Q. T. P., Tran, L. D., Nguyen, C., Vo, D.-V. N., Do, S. T., 2018. Effective photocatalytic activity of mixed Ni/Fe-base metal-organic framework under a compact fluorescent daylight lamp. Catalyst. 8(11), 487. https://doi.org/10.3390/catal8110487

Patel, S. K. S., Lee, J.-K., Kalia, V. C., 2018. Nanoparticles in biological hydrogen production: an overview. Indian J. Microbiol. 58, 8–18. https://doi.org/10.1007/s12088-017-0678-9

Rafiee, M., Bashiri, H., 2020. Application of response surface methodology and dynamic Monte Carlo simulation to study the hydrogen production from formic acid on Ni (1 0 0). Mater. Sci. Eng. B. 262, 114729. https://doi.org/10.1016/j.mseb.2020.114729

Rambabu, K., Bharath, G., Banat, F., Hai, A., Show, P. L., Nguyen, T. H. P., 2021. Ferric oxide/date seed activated carbon nanocomposites mediated dark fermentation of date fruit wastes for enriched biohydrogen production. Int. J. Hydrog. Energy, 46(31), 16631–16643. https://doi.org/10.1016/j.ijhydene.2020.06.108

Ramprakash, B., Incharoensakdi, A., 2020. Light-driven biological hydrogen production by Escherichia coli mediated by TiO2 nanoparticles. Int. J. Hydrog. Energy, 45(11), 6254–6261. https://doi.org/10.1016/j.ijhydene.2020.01.011

Rhazi, N., Hannache, H., Oumam, M., Sesbou, A., Charrier, B., Pizzi, A., Charrier-El Bouhtoury, F., 2019. Green extraction process of tannins obtained from Moroccan Acacia mollissima barks by microwave: Modeling and optimization of the process using the response surface methodology RSM. Arab. J. Chem. 12(8), 2668–2684. https://doi.org/10.1016/j.arabjc.2015.04.032

Rittmann, S., Herwig, C., 2012. A comprehensive and quantitative review of dark fermentative biohydrogen production. Microb. Cell Factories, 11, 1–18. https://doi.org/10.1186/1475-2859-11-115

Salarian, A.-A., Hami, Z., Mirzaei, N., Mohseni, S. M., Asadi, A., Bahrami, H., Vosoughi, M., Alinejad, A., Zare, M.-R., 2016. N-doped TiO_2 nanosheets for photocatalytic degradation and mineralization of diazinon under simulated solar irradiation: Optimization and modeling using a response surface methodology. J. Mol. Liq. 220, 183–191. https://doi.org/10.1016/j.molliq.2016.04.060

Shekari, H., Sayadi, M. H., Rezaei, M. R., Allahresani, A., 2017. Synthesis of nickel ferrite/titanium oxide magnetic nanocomposite and its use to remove hexavalent chromium from aqueous solutions. Surf. Interfaces, 8, 199–205. https://doi.org/10.1016/j.surfin.2017.06.006

Sigal, A., Leiva, E. P. M., Rodríguez, C. R. (2014). Assessment of the potential for hydrogen production from renewable resources in Argentina. Int. J. Hydrog. Energy, 39(16), 8204–8214. https://doi.org/10.1016/j.ijhydene.2014.03.157

Song, W., Ding, L., Liu, M., Cheng, J., Zhou, J., Li, Y.-Y., 2020. Improving biohydrogen production through dark fermentation of steam-heated acid pretreated Alternanthera philoxeroides by mutant Enterobacter aerogenes ZJU1. Sci. Total Environ. 716, 134695. https://doi.org/10.1016/j.scitotenv.2019.134695

Srivastava, N., Srivastava, M., Malhotra, B. D., Gupta, V. K., Ramteke, P. W., Silva, R. N., Shukla, P., Dubey, K. K., Mishra, P. K., 2019. Nanoengineered cellulosic biohydrogen production via dark fermentation: a novel approach. Biotechnol. Adv. 37(6), 107384. https://doi.org/10.1016/j.biotechadv.2019.04.006

Tasleem, S., Tahir, M., Khalifa, W. A., 2021. Current trends in structural development and modification strategies for metal-organic frameworks (MOFs) towards photocatalytic H_2 production: a review. Int. J. Hydrog. Energy, 46(27), 14148–14189. https://doi.org/10.1016/j.ijhydene.2021.01.162

Tiang, M. F., Hanipa, M. A. F., Abdul, P. M., Jahim, J. M., Mahmod, S. S., Takriff, M. S., Lay, C.-H., Reungsang, A., Wu, S.-Y., 2020. Recent advanced biotechnological strategies to enhance photo-fermentative biohydrogen production by purple non-sulphur bacteria: an overview. Int. J. Hydrog. Energy, 45(24), 13211–13230. https://doi.org/10.1016/j.ijhydene.2020.03.083

Trchounian, K., Blbulyan, S., Trchounian, A., 2013. Hydrogenase activity and proton-motive force generation by Escherichia coli during glycerol fermentation. J. Bioenerg. Biomembr. 45(3), 253–260. https://doi.org/10.1007/s10863-012-9493-0

Xia, A., Jacob, A., Herrmann, C., Murphy, J. D., 2016. Fermentative bio-hydrogen production from galactose. Energy, 96, 346–354. https://doi.org/10.1016/j.energy.2015.12.087

Xu, X., Li, Y., Zhang, G., Yang, F., He, P., 2019. NiO-$NiFe_2O_4$-rGO magnetic nanomaterials for activated peroxymonosulfate degradation of Rhodamine B. Water, 11(2), 384. https://doi.org/10.3390/w11020384

Yi, L., Wang, L., Guo, L., Jin, H., Cao, W., Xu, J., Wei, W., 2021. Molecular dynamic study on hydrogen production from unsymmetrical dimethylhydrazine in supercritical water. J. Mol. Liq. 339, 117051. https://doi.org/10.1016/j.molliq.2021.117051

Yin, Y., Wang, J., 2019. Enhanced biohydrogen production from macroalgae by zero-valent iron nanoparticles: Insights into microbial and metabolites distribution. Bioresour. Technol. 282, 110–117. https://doi.org/10.1016/j.biortech.2019.02.128

Zhang, J., Li, W., Yang, J., Li, Z., Zhang, J., Zhao, W., Zang, L., 2021. Cobalt ferrate nanoparticles improved dark fermentation for hydrogen evolution. J. Clean. Prod. 316, 128275. https://doi.org/10.1016/j.jclepro.2021.128275

Zhang, Y., Shen, J., 2007. Enhancement effect of gold nanoparticles on biohydrogen production from artificial wastewater. Int. J. Hydrog. Energy, 32(1), 17–23. https://doi.org/10.1016/j.ijhydene.2006.06.004

Ziara, R. M. M., Miller, D. N., Subbiah, J., Dvorak, B. I., 2019. Lactate wastewater dark fermentation: the effect of temperature and initial pH on biohydrogen production and microbial community. Int. J. Hydrog. Energy, 44(2), 661–673. https://doi.org/10.1016/j.ijhydene.2018.11.045

Credit Author Statement

Nazanin Fahoul: Conceptualization, Data curation, Formal analysis, Investigation, Methodology, Visualization, Writing – original draft

Mohammad Hossein Sayadi: Conceptualization, Funding acquisition, Project administration, Resources, Supervision, Writing – review & editing.

Mohammad Reza Rezaei: Methodology, Formal analysis, Investigation, Methodology, Visualization

Shahin Homaeigohar: Visualization, Conceptualization, Investigation, Writing – review & editing.

Graphical abstract

$$\mathbf{NPs} + \boldsymbol{O_2} \rightarrow \boldsymbol{ROS}\ (\boldsymbol{O_2^{\circ -}} + \boldsymbol{H_2O_2})$$

$$\mathbf{C_6H_{12}O_6 + 4H_2O \rightarrow 4H_2 + 2CH_3COOH + 2CO_2 \quad (\Delta G_0 = -206\ kJ)}$$

$$\mathbf{C_6H_{12}O_6 + 2H_2O \rightarrow 2H_2 + CH_3CH_2CH_2COOH + 2CO_2\ (\Delta G_0 = -254\ kJ)}$$

$$\mathbf{C_6H_{12}O_6 + 3H_2O \rightarrow CH_3OO^- + 2HCO_3^- + 3H^+ + CH_3CH_2OH \quad (\Delta G_0 = -97\ kJ/mol)}$$

Highlights

- Real dairy wastewater are used for biohydrogen production.
- Activated sludge is applied as a novel carbon source and a novel microbial community
- Implementing the Central Composite Design model from the response surface models
- The $NiFe_2O_4$ nanoparticles could properly act as a catalyst for the dark fermentation process